DALTON
FULL PAPER

Crystallisation of H_3BTC, H_3TPO or H_2SDA with M^{II} (M = Co, Mn or Zn) and 2,2′-bipyridyl: design and control of co-ordination architecture, and magnetic properties (H_3BTC = benzene-1,3,5-tricarboxylic acid, H_3TPO = tris(4-carboxylphenyl)phosphine oxide, H_2SDA = *cis*-stilbene-4,4′-dicarboxylic acid) †

M. John Plater,*[a] Mark R. St. J. Foreman,[a] Eugenio Coronado,*[b] Carlos J. Gómez-García[b] and Alexandra M. Z. Slawin[c]

[a] *Department of Chemistry, University of Aberdeen, Meston Walk, Aberdeen, UK AB24 3UE. E-mail: m.j.plater@abdn.ac.uk; Fax:Int. code +44 1224 272921*
[b] *Department Quimica Inorganica, Universidad de Valencia, 46100 Burjassot, Spain. E-mail: eugenio.coronado@uv.es; Fax: Int. code +34 96 3864859*
[c] *Molecular Structure Laboratory, Department of Chemistry, University of St. Andrews, St. Andrews, Fife, UK KY16 9ST. E-mail: amzs@st-andrews.ac.uk*

Received 2nd July 1999, Accepted 5th October 1999

The hydrothermal reaction of benzene-1,3,5-tricarboxylic acid (H_3BTC) with M^{II} (M = Mn, Co or Zn), tris(4-carboxyphenyl)phosphine oxide (H_3TPO) or *cis*-stilbene-4,4′-dicarboxylic acid (H_2SDA) with Co^{II} and 2,2′-bipyridyl (BIPY) gave 1-D co-ordination networks formulated as: [M(HBTC)(BIPY)(H_2O)] (M = Mn **1**, Co **2**, or Zn **3**; $[Co_3(BTC)_2(BIPY)_2(H_2O)_6]\cdot 4H_2O$ **4**, $[Co_3(TPO)_2(BIPY)_2(H_2O)_6]\cdot xH_2O$ **5** and [Co(SDA)(BIPY)(H_2O)] **6**. Structures **1** and **2** consist of double stranded chains of alternating HBTC dianions and dimeric units M^{II}–M^{II} linked by two μ-(1,1) bridging carboxylates. Magnetic properties of **1** and **2** indicate the presence of ferromagnetic exchange interactions within the dimers. Structures **4** and **5** consist of chains with a molecular ladder motif which are stacked creating large channels lined by hydrated cobalt(II) ions. The H_2O/D_2O solvent exchange in structure **5**, studied by infrared spectroscopy and thermal gravimetric analysis–mass spectrometry, provides evidence for the porosity and zeolitic nature of the material.

Introduction

The solid state assembly of open framework metal–organic co-ordination polymers is attracting increasing attention owing to the potential discovery of novel functional materials which are expected to find applications in catalysis, non-linear optics, magnetism, sensors and molecular recognition.[1] Understanding and controlling the factors which govern the assembly process and lattice stability is critical to technological developement. Such factors include the formation of 1-D, 2-D or 3-D co-ordinative networks, the formation of interpenetrating lattices *versus* the inclusion of solvent or guest molecules, lattice stability to guest or solvent exchange or removal and re-absorption, counter ion mobility for ion exchange, pore volume and accessibility of co-ordinatively unsaturated metal centres and assemblies which propagate magnetic interactions between paramagnetic metal ions.[2] One approach to novel porous networks involves the reaction of benzene-1,3,5-tricarboxylic acid (H_3BTC) with alkaline earths (M = Ca, Sr or Ba)[3] or transition metal ions (M = Co, Zn or Ni) under hydrothermal conditions.[4] This gives co-ordination polymers containing the $HBTC^{2-}$ dianion or the BTC trianion respectively and the hydrated metal ion. Anion H_2BTC^- has not yet formed under these conditions. In search of a further class of materials of this type we have investigated the influence of the bidentate ligand 2,2′-bipyridyl upon co-ordination architecture during the assembly of aromatic acids with metal ions (M = Co, Mn or Zn). It was predicted that this ligand would favour the formation of 1-D co-ordinative chains, such as the possible chain shown in Fig. 1, by reducing the available metal-ion binding sites that might have led to polymer growth in other directions. The chains shown are desirable because they possess pockets that might give the compound porous properties. The edge bipyridyl ligands were expected to create pockets allowing adjacent chains to interweave and associate by van der Waals forces or π stacking.[5]

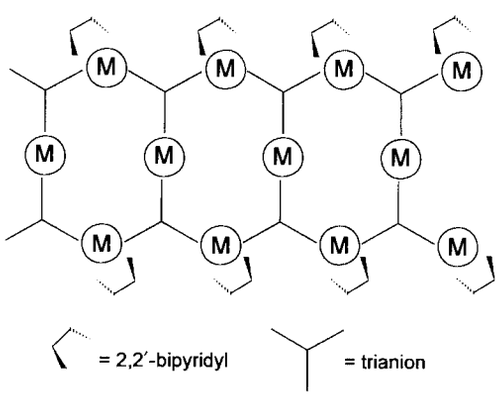

Fig. 1 Drawing of a possible 1-D infinite co-ordinative chain with the metal cations along the edges capped by a bis-donor ligand such as 2,2′-bipyridyl.

† *Supplementary data available*: rotatable 3-D crystal structure diagram in CHIME format. See http://www.rsc.org/suppdata/dt/1999/4209/

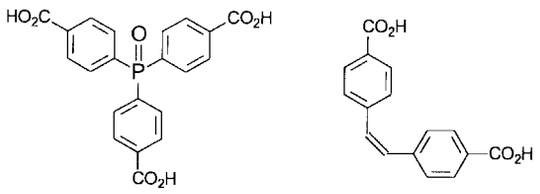

H_3TPO H_2SDA

Results and discussion

In this paper we report the hydrothermal synthesis and X-ray structural characterisation[6] of crystalline solids prepared from (i) H_3BTC and acetates of Mn^{II}, Co^{II} and Zn^{II} with 2,2′-bipyridyl, (ii) tris(4-carboxylphenyl)phosphine oxide (H_3TPO) and *cis*-stilbene-4,4′-dicarboxylic acid (H_2SDA) with cobalt(II) acetate and 2,2′-bipyridyl. Table 1 gives a summary of the crystallographic data and Table 2 summarises key hydrogen bond lengths and angles. Hydrothermal synthesis of H_3BTC with the acetate of Mn^{II}, Co^{II}, or Zn^{II} and 2,2′-bipyridyl in the ratio of 1 : 1 : 1 gives solids **1**, **2** and **3** respectively which possess a similar asymmetric unit shown in Fig. 2. The same numbering scheme has been used for each. All 3 compounds have the same molecular formula but each has a different structure presumably as a consequence of the preferred metal ion co-ordination environment. As expected each structure has an infinite co-ordinative network in one dimension only. Networks **1** and **2** formulated as [M(HBTC)(BIPY)(H_2O)] where M = Mn or Co respectively consist of similar double stranded chains of alternating HBTC dianions and dimeric units M^{II}–M^{II} linked by two bridging oxygens coming from two carboxylate ligands (Figs. 3 and 4). The metal ions each possess a distorted octahedral geometry and are co-ordinated by one bipyridyl ligand, one monodentate carboxylate ion, two bifurcated carboxylate anions and one water molecule. For each HBTC dianion one carboxylate anion oxygen is monodentate and the other carboxylate anion forms a bifurcated bridge between the two metal ions. The chains of M_2O_2 squares are bridged by two HBTC dianions forming 16 membered metallocyclic rings.

For structure **1** the Mn · · · Mn internuclear distance is 3.5 Å and the chains run parallel to the *b* axis (Fig. 3). The HBTC anions are stacked in pairs about 3.35 Å apart which corresponds to the van der Waals distance between them. The angle O–Mn–O between the 2 bridging oxygen atoms in the Mn_2O_2 ring is 74.9° while the Mn–O–Mn angle in the ring is 105.1°.

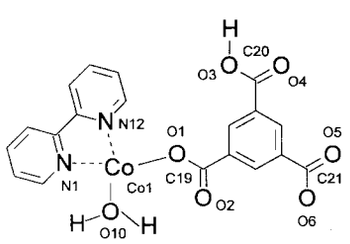

Fig. 2 Drawing of the asymmetric unit for structures **1**–**3**.

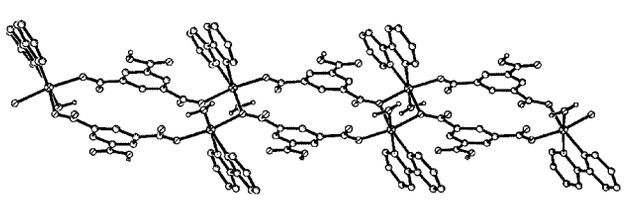

Fig. 3 Ball and stick drawing of the double stranded chains in compound **1**. Selected bond lengths [Å] and angles [°]: Mn1 · · · Mn1 3.5, Mn1–O10 2.133(2), Mn1–N12 2.302(2), Mn1–N1 2.229(2), Mn1–O1 2.2172(12), Mn1–O1″ 2.2003(12) and Mn1–O5′ 2.1524(12); Mn1″–O1–Mn1 105.11(5) and O1″–Mn1–O1 74.88(5).

The N–Mn–N angle of bound bipy is 71.9°. The monodentate carboxylate oxygen (O5) is *cis* to both BIPY nitrogen atoms, while the water oxygen is *trans* to one nitrogen. The undeprotonated carboxylic acid groups C20 point in opposite directions approximately along the *a* axis. The chains are stabilised by one intrachain and two interchain hydrogen bonds. The same hydrogen bonding motif occurs in structures **1**–**3** and is shown in Fig. 5. Each carboxylic acid acts as a hydrogen bond donor and acceptor. Atom H3O of carboxylic acid group C20 forms an interchain hydrogen bond (1.72 Å) to O2‴ of the monodentate carboxylate group C19; H10B of the water molecule O10 forms an interchain hydrogen bond (1.82 Å) to O4″ of carboxylic group C20 completing a 10-membered ring. The remaining proton H10A of the water molecule O10 forms an intrachain hydrogen bond (1.75 Å) to O6′ of the bifurcated carboxylate anion C21 completing a 6-membered ring. The interchain and intrachain hydrogen bonding is clearly visible in the packing diagram shown for compound **2** in Fig. 4 (bottom) and in Fig. 5. The hydrogen bonds present are all quite strong since they are shorter than the average length for a hydrogen bond which is typically in the range 1.9–2.1 Å. Hydrogen bonding is

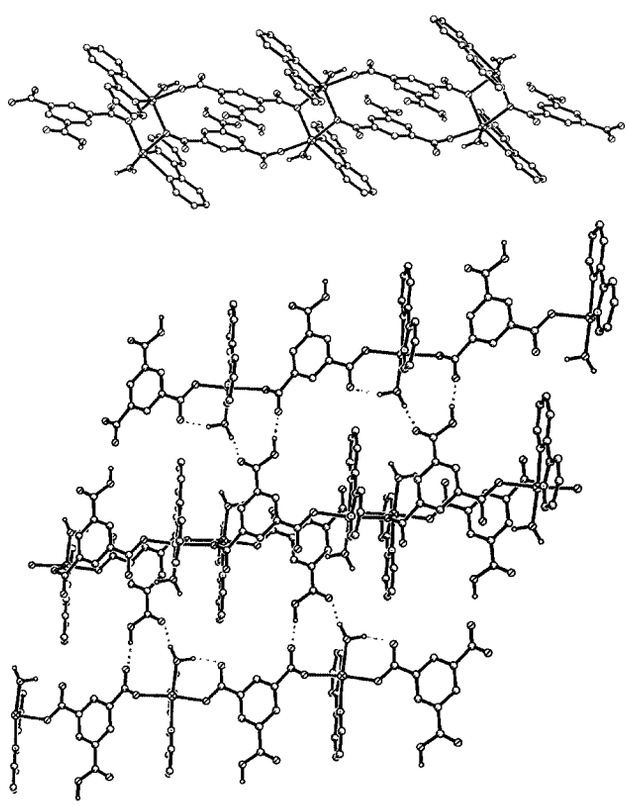

Fig. 4 Top: ball and stick drawing of the double stranded chains in compound **2**. Bottom: Packing diagram illustrating the interchain hydrogen bonding network. Selected bond lengths [Å] and angles [°]: Co1 · · · Co1 3.37, Co1–O10 2.062(2), Co1–N12 2.106(2), Co1–N1 2.140(2), Co1–O1 2.074(2), Co1–O5′ 2.130(2) and Co1–O5″ 2.171(2); Co1‴–O5–Co1″ 102.94(6), O1–Co1–O5′ 164.53(6) and O1–Co1–O5″ 87.93(6).

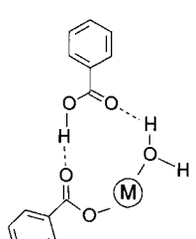

Fig. 5 Drawing showing the interchain hydrogen bonding present between co-ordinative chains in structures **1**–**3**.

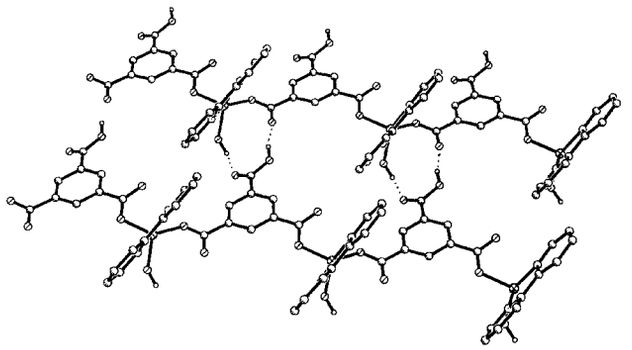

Fig. 6 Packing diagram illustrating the single stranded chains and interchain hydrogen bonding network in compound **3**. Selected bond lengths [Å]: Zn1–O1 1.962(2), Zn1–O10 2.112(2), Zn1–N1 2.164(3), Zn1–N12 2.118(2) and Zn1–O5′ 2.016(2).

probably an important factor in the supramolecular assembly and stabilisation of the lattice.

For structure **2** the Co · · · Co internuclear distance is 3.37 Å and the chains run parallel to the *c* axis. The obvious variation from octahedral geometry are angles N–Co–N (76.7°) and O5–Co–O5 (77.1°) of the 4-membered ring. The Co–O–Co angle is 102.9°. The water oxygen (O10) is *trans* to one of the BIPY nitrogen atoms while O2 is *cis* to both nitrogens. The chains are stabilised by one intrachain and two interchain hydrogen bonds analogous to the structure of **1** although the hydrogen bonds exist between different atoms. Atom H3O of the carboxylic acid group C20 forms an interchain hydrogen bond of length 1.62 Å to O6′ of the bifurcated carboxylate anion C21; H10A of the water molecule O10 forms an interchain hydrogen bond (1.80 Å) to O4″ of carboxylate group C20. The remaining proton H10B of the water molecule O10 forms an intrachain hydrogen bond (1.71 Å) to O2 of monodentate carboxylate anion C19 completing a 6-membered ring (see Fig. 6).

Compound **3** formulated as [Zn(HBTC)(BIPY)(H_2O)] consists of single stranded chains of alternating HBTC dianions and zinc(II) cations running parallel to the *a* axis (Fig. 6). The cations are co-ordinated by two monodentate carboxylate anions, one bipyridyl group and one water molecule, and adopt a distorted square based pyramidal geometry. Owing to the fact that Zn^{II} has a d^{10} electron configuration and lacks crystal field stabilisation energy, the co-ordination of ligands around Zn is likely to be controlled by steric effects. The chains are stabilised by three interchain hydrogen bonds. Atom H30 of carboxylic acid group C20 forms a hydrogen bond (1.63 Å) to O6‴ of carboxylate anion C21. Proton H10C of the water molecule O10 forms a hydrogen bond (1.84 Å) to O4″ of carboxylate anion C20 completing a 10-membered ring. This can be seen in the packing diagram in Fig. 6. The other proton of the water molecule H10B forms a hydrogen bond (1.99 Å) to O5′ of carboxylate anion C21 in an adjacent layer. This hydrogen bond is longer and weaker than the others owing to the co-ordination of O5′ to a zinc(II) cation.

The phase shown in Fig. 1 would have a different stoichiometry to the above structures of composition M : HBTC : BIPY (1 : 1 : 1). The synthesis was repeated using Co : H_3BTC : BIPY in a 1.5 : 1 : 1 ratio. Two different phases could be identified by visual examination of the red crystalline material. By carefully selecting similar looking red crystals a material of approximate composition $[Co_3(BTC)_2(BIPY)_2(H_2O)_6]\cdot xH_2O$ **4** ($x \approx 2$) was identified by microanalysis. The single crystal structure was determined which showed that the lattice motif described in the introduction had been formed. Fig. 7 shows a drawing of the asymmetric unit and the infinite double stranded chains which run along the *a* axis in the *ac* plane. The lattice contains two different cobalt(II) cations. Those down the centre connecting the chains together are octahedral and are co-ordinated by two *trans* monodentate carboxylate anions and four water

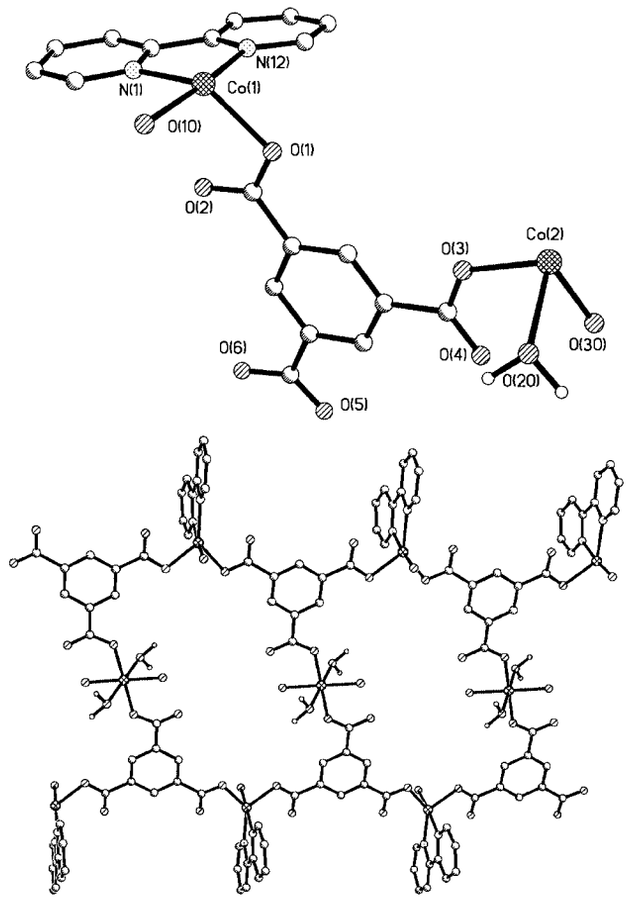

Fig. 7 Top: ball and stick drawing of the asymmetric unit in compound **4**. Bottom: drawing of a double stranded chain. Selected bond lengths [Å]: Co1–O1 2.068(3), Co1–O10 2.096(3), Co1–N1 2.101(3), Co1–N12 2.119(3), Co1–O5′ 2.116(3), Co2–O3‴ 2.052(3), Co2–O30‴ 2.093(3) and Co2-O20‴ 2.146(3).

molecules. Those along the edges are five-co-ordinated by two monodentate carboxylate anions, one bipyridyl group and one water molecule. The bipy nitrogens, Co and water oxygens are approximately coplanar possessing a N12–N1–Co1–O10 torsion angle of −178.6°. The carboxylate oxygens are out of this plane with torsion angles N12–N1–Co1–O1 of −76.5° and N12–N1–Co1–O5 of 76.1°. While the common co-ordination geometries for Co^{II} are octahedral and tetrahedral, examples of trigonal bipyramidal complexes are known. The structure resembles a molecular ladder made up of edge sharing 32-membered rhombohedra. The hydrogen atoms of water molecules O10 and O30 could not be located. The hydrogen atoms H20 of water molecule O20 which is co-ordinated to Co2 were located: H20A forms a hydrogen bond (1.75 Å) to O2′ of an adjacent double strand as does H20B but on the opposite side. Two non-co-ordinated water molecules per asymmetric unit were found in four different locations indicative of the free volume created in the lattice by the co-ordinative network. This amounts to the inclusion of four disordered water molecules for each rhombohedra ($x = 4$ in **4**). The double strands are stacked in a slightly staggered arrangement along the *b* axis forming an open framework lattice with molecular channels. However, owing to the difficulty of obtaining this material as a pure phase further studies on its porosity were not carried out.

Owing to the success of crystallising networks from H_3BTC, divalent metal ions and 2,2′-bipyridyl it was of interest to investigate the crystallisation of networks from different aromatic carboxylic acids. Two further acids were studied namely H_3TPO[7] and H_2SDA. Heating H_3TPO with $Co(OAc)_2$ and 2,2′-bipyridyl in water gave a red crystalline material of formula

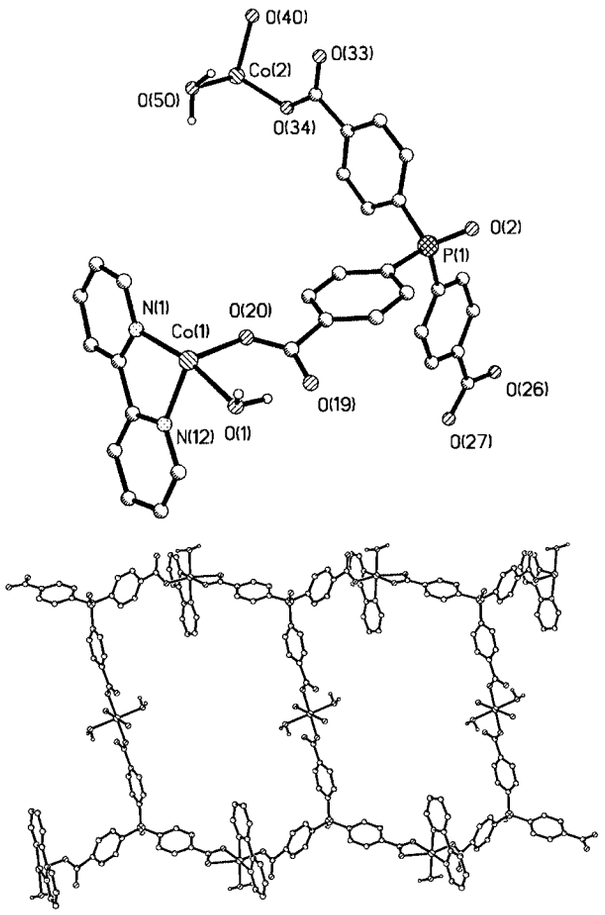

Fig. 8 Top: ball and stick drawing of the asymmetric unit in compound **5**. Bottom: drawing of a double stranded chain. Selected bond lengths [Å]: Co1–O20 2.056(4), Co1–O1 2.095(5), Co1–O26′ 2.094(5), Co1–N1 2.114(5), Co1–N12 2.103(5), Co1–O27′ 2.317(5), Co2–O34‴ 2.054(6), Co2–O40‴ 2.101(6) and Co2–O50‴ 2.149(6).

$[Co_3(TPO)_2(BIPY)_2(H_2O)_6]$ **5** determined by microanalysis after drying under vacuum. The single crystal structure consists of infinite double stranded chains in one dimension which resemble a molecular ladder (Fig. 8). In this respect it is similar to the previously predicted BTC derived lattice found in compound **4**. There are two different cobalt cations in the network. Those along the edges adopt a distorted octahedral environment and are co-ordinated by one monodentate carboxylate anion, one bidentate carboxylate anion, one bipyridyl ligand and one water molecule. In common with structures **1** and **2** the water (O1) is *trans* to one of the bipy nitrogens; O27 is 2.32 Å from the cobalt while the other carboxylate oxygens are all within 2.1 Å. Angle O26–Co1–O27 is 59.9° and N1–Co1–N12 is 77.6°. The physical constraints of assembling the lattice probably force O27 to be removed from the ideal octahedral position. The cobalt cations connecting the strands are octahedrally co-ordinated by 4 water molecules and 2 *trans* carboxylate anions. The hydrogen atoms of two of these waters (O40) could not be located. Hydrogen H1B of the water O1 forms an intrachain hydrogen bond (1.68 Å) to O19 completing a 6-membered ring; H1A of the water O1 forms an interchain hydrogen bond (1.77 Å) to the oxygen O2′ of the phosphine oxide. Non-co-ordinating, disordered water molecules were observed which were absent according to microanalytical data. The sample used for microanalysis had been dried under vacuum whereas that for crystallography was taken from water. This suggests that the water is loosely bound and can escape from the porous structure very easily. This is supported by thermal gravimetric analysis of an as synthesized sample which showed ready loss in mass immediately at 25 °C. Between 40 and 170 °C three overlapping endothermic mass losses totalling 9.6% occurred. The conversion of the octahydrate into an anhydrous solid requires a mass loss of 10% which indicates the presence of at least two non-co-ordinating water molecules. The structural integrity of the porous framework is maintained after room temperature desorption of the non-co-ordinating water molecules, because powder diffraction patterns of the as synthesized and evacuated material are sharp and identical. The framework is probably able to maintain its shape or crystallinity and support internal void volume because water molecules have not been removed from the metal-ion co-ordination sphere which can therefore maintain its geometry. Full crystallographic characterisation of the porous solvated and desolvated (−EtOH) molecular framework co-ordination polymer $[Ni(bipy)_{1.5}(NO_3)_2]\cdot EtOH$ was also reported recently.[8] In this structure the EtOH molecules are not bound in the metal ion co-ordination sphere. Standing a sample of undried material in heavy water for 3 d showed that solvent exchange had occurred as evidenced by the appearance of a broad O–D absorption at 2493 cm^{-1}. The infrared spectrum was identical to that of a sample prepared in D_2O. The exchange of H_2O for D_2O was also studied by TG-MS. This showed the presence of some D_2O, DHO and H_2O indicating that complete exchange of all the included H_2O for D_2O had not occurred. Non-co-ordinated H_2O would presumably exchange the fastest by diffusion whereas co-ordinated H_2O molecules would probably exchange more slowly. The H_2O/D_2O exchange illustrates the porous nature of the framework. Attempted H_2O/D_2O exchange on unevacuated samples of the previously reported porous solids $[Ca(HBTC)(H_2O)]\cdot H_2O$[3] and $[Co_3(BTC)_2(H_2O)_{12}]$[4a] was unsuccessful which illustrates the improved porosity of the new TPO solid.

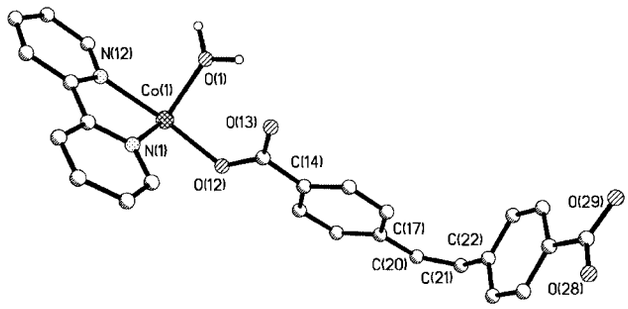

Fig. 9 Ball and stick drawing of the asymmetric unit in compound **6**. Selected bond lengths [Å]: Co1–O12 2.039(2), Co1–O1 2.085(2), Co1–O29′ 2.103(2), Co1–O28′ 2.504(3), Co1–N1 2.147(2) and Co1–N12 2.137(2).

The formation of co-ordination polymers from the ligand H_2SDA was of interest owing to its existence as *cis* and *trans* isomers. Either isomer or a mixture of both might give networks. Heating a commercially available sample, which consisted of a mixture of *cis* and *trans* isomers, with $Co(OAc)_2$ and 2,2′-bipyridyl in water gave a red crystalline material of composition $[Co(SDA)(BIPY)(H_2O)]$ **6** which was admixed with some unchanged ligand. This suggested that only one isomer had formed a co-ordination polymer. The unchanged ligand was removed by washing with ethanol. The crystal structure consists of infinite single stranded chains of *cis*-SDA running along the *b* axis (Fig. 9). The cobalt(II) cations are co-ordinated by one monodentate carboxylate anion, one bidentate carboxylate anion, one bipyridyl ligand and one water molecule. One of the *cis*-SDA aromatic rings is conjugated to the alkene group with a torsion angle of 3.6° (C17–C20–C21–C22) while the other is twisted out of the plane of the alkene π system at an angle of 90° (C20–C21–C22–C23). Atom H1B of the water molecule O1 forms an intrachain bifurcated hydrogen bond between O13′ (2.10 Å) and O28′ (2.22 Å); H1A of the water molecule O1 forms an interchain hydrogen bond to

Table 1 Summary of crystal data for compounds **1**–**6**

	1	**2**	**3**	**4**	**5**	**6**
Formula	$C_{19}H_{14}MnN_2O_7$	$C_{19}H_{14}CoN_2O_7$	$C_{19}H_{14}N_2O_7Zn$	$C_{19}H_{25}Co_{1.5}N_2O_{11}$	$C_{62}H_{54}Co_3N_4O_{21}P_2$	$C_{26}H_{20}CoN_2O_5$
M_r	437.26	441.25	447.69	545.80	1429.82	499.37
T/K	293	293	293	293	293	293
Crystal system	Monoclinic	Triclinic	Triclinic	Triclinic	Triclinic	Monoclinic
Space group	$P2_1/n$	$P\bar{1}$	$P\bar{1}$	$P\bar{1}$	$P\bar{1}$	$P2_1/a$
a/Å	10.364(3)	9.560(5)	9.462(10)	10.044(7)	10.910(10)	11.238(10)
b/Å	10.504(10)	10.114(5)	9.482(2)	10.341(7)	11.437(11)	13.552(2)
c/Å	17.083(4)	10.836(5)	11.462(3)	12.109(9)	13.716(13)	14.579(3)
α/°		98.55(10)	111.95	74.719(2)	110.791(2)	
β/°	103.3090(10)	111.59 (10)	93.091(10)	74.947(2)	93.6520(10)	94.4970(10)
γ/°		104.92(10)	101.878(10)	79.909(2)	99.355(2)	
V/Å^3	1810	906	923.58(3)	1163.98(14)	1565.1(3)	2213.45(6)
Z	4	2	2	2	1	4
Reflections collected	10478	4373	4015	7104	9933	9617
Independent reflections	4074	2596	2627	5190	7016	3190
Reflections observed	4024	2546	2577	5140	7016	3135
R(int)	0.0306	0.0345	0.0399	0.0950	0.0358	0.0288
Final R [$I > 2\sigma(I)$]	0.0314	0.0284	0.0295	0.0482	0.0736	0.0327
Final $wR2$	0.0670	0.0632	0.0767	0.0938	0.1997	0.0781

Table 2 Summary of hydrogen bond lengths and angles

Compound	O	H	X	H···X/Å	O···X/Å	O–H···X/°
1 [Mn(HBTC)(BIPY)(H_2O)]	O3	H30	O2‴	1.72	2.66	173
	O10	H10B	O4″	1.82	2.72	173
	O10	H10A	O6′	1.75	2.61	164
2 [Co(HBTC)(BIPY)(H_2O)]	O3	H30	O6′	1.62	2.59	169
	O10	H10A	O4″	1.80	2.78	172
	O10	H10B	O2	1.71	2.63	156
3 [Zn(HBTC)(BIPY)(H_2O)]	O3	H30	O6‴	1.63	2.58	164
	O10	H10C	O4″	1.84	2.77	156
	O10	H10B	O5′	1.99	2.84	144
4 $[Co_3(BTC)_2(BIPY)_2(H_2O)_6]\cdot 4H_2O$	O20	H20A	O2′	1.75	2.71	165
	O20	H20B	O50	1.92	2.75	165
5 $[Co_3(TPO)_2(BIPY)_2(H_2O)_6]\cdot xH_2O$	O1	H1A	O2′	1.77	2.74	176
	O1	H1B	O19	1.68	2.64	169
6 [Co(SDA)(BIPY)(H_2O)]	O1	H1A	O12	1.90	1.90	175
	O1	H1B	O13′	2.10	2.10	120
	O1	H1B	O28′	2.22	2.22	130

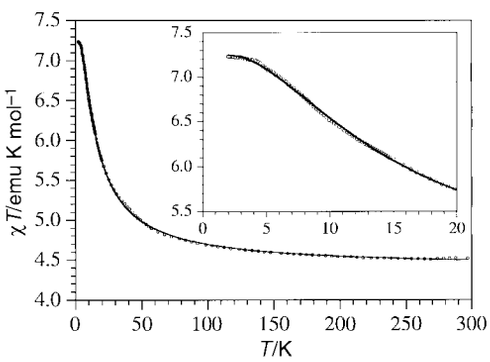

Fig. 10 Thermal dependence of the product susceptibility times the temperature (χT) for complex **1** (○) and the theoretical behaviour of a ferromagnetic manganese(II) dimer (—). The inset shows the plateau of χT in the low temperature region.

O12 of a monodentate carboxylate anion in an adjacent layer. The separation of the stilbene isomers illustrates an example of hydrothermal synthesis in which a single diastereomer is recognised and selectively crystallised from a mixture into a co-ordination network. This might have practical applications for some separations.

Magnetic properties

The magnetic properties of the manganese(II) compound **1** are depicted in Fig. 10 with a plot of the product χT (proportional to the square of the magnetic moment) *vs.* temperature. At room temperature the χT value is *ca.* 4.7 emu K per manganese, which is close to the value expected for magnetically isolated manganese(II) centres possessing a spin sextuplet $S = 5/2$. Upon cooling χT reveals a continuous increase with a tendency of levelling below 5 K, reaching a value of 7.25 emu K mol^{-1} at 1.8 K. Such a behaviour is characteristic of a ferromagnetic coupling between two spin sextuplets, whereby the plateau at lower temperature corresponds to the exclusive thermal population of the $S = 5$ ground spin state. Therefore, the magnetic data were conveniently analysed with the appropriate van Vleck equation for the magnetic susceptibility of a high spin manganese(II) dimer with the isotropic Heisenberg hamiltonian $H_{ex} = -2JS_A\cdot S_B$, where J is the magnetic coupling parameter. A fitting of the data to this model leads to $J = 0.90$ cm^{-1} and $g = 2.0$; 9% of monomeric impurity had to be introduced. The agreement is excellent in the whole temperature range (Fig. 10). These results indicate that although the structure of this compound consists of a double chain of dimers connected through two HBTC bridging ligands, the exchange interaction is restricted to the Mn^{II}–Mn^{II} pairs which are magnetically coupled through two bridging oxygens from two carboxylate groups. In this case the spin coupling through the HBTC bridging ligands is quite negligible, in agreement with the fact that these anions keep the manganese(II) ions at a distance as large as 9 Å. An additional proof of this picture comes from the low temperature magnetisation data. Thus, the isothermal variation of the magnetisation at 2 and 5 K *vs.* the applied magnetic field closely follows the behaviour expected for a total

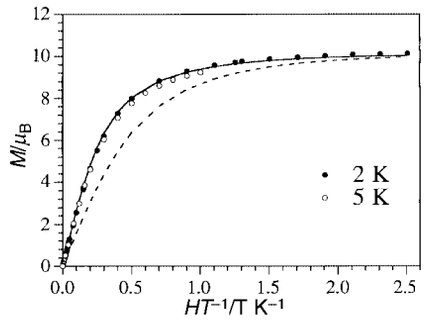

Fig. 11 Plot of the isothermal magnetisation M (per pair of manganese(II) ions) *vs.* H/T at 2 and 5 K for complex **1**. The Brillouin function for a spin $S = 5$ with $g = 2.0$ is plotted as a solid line and compared to the behaviour calculated for two non-interacting local spins $S_A = S_B = 5/2$ (—).

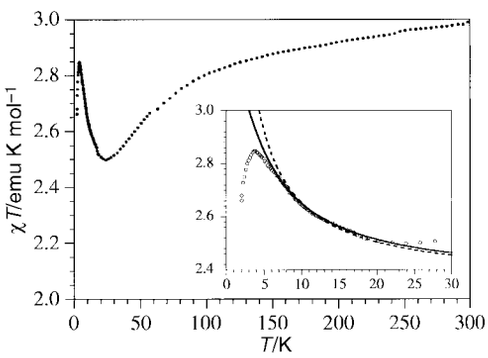

Fig. 12 Thermal dependence of the product susceptibility times the temperature (χT) for complex **2** (○). In the inset the best fits of the data in the low temperature region by an anisotropic exchange dimeric model are plotted as solid ($J_{xy}/J_z = 1$) and dashed ($J_{xy}/J_z = 2$) lines.

spin $S = 5$ with $g = 2.0$, indicating that the ground spin state of the system is the ferromagnetic one (Fig. 11). The curve lies well above that for two uncoupled local spins $S = 5/2$ (dashed line in Fig. 11). The fact that at two different temperatures (2 and 5 K) the curves of M *vs.* H/T are coincidental, within the experimental error, is conclusive evidence of the good magnetic insulation of these ferromagnetic dimers.

The magnetic properties of the analogous cobalt(II) derivative **2** are depicted in Fig. 12. Upon cooling the χT product shows a continuous decrease from 3 emu K mol^{-1} at 300 K to 2.5 emu K mol^{-1} at 25 K where a rounded minimum is observed. Below this temperature χT increases and reaches a sharp maximum at *ca.* 4 K. This behaviour can be qualitatively explained if we bear in mind that high-spin octahedral Co^{II} has an orbitally degenerate ground state $^4T_1$. Thus, the decrease in χT down to 25 K basically corresponds to a single-ion behaviour. It accounts for the splitting of the $^4T_1$ term into six Kramers doublets as a consequence of the combined effect of spin–orbit coupling and distortion from octahedral symmetry.[9] However, the observed increase in χT below this temperature is no longer coming from the single-ion behaviour but rather from a ferromagnetic Co^{II}–Co^{II} exchange interaction. More precisely, it reflects a ferromagnetic coupling between two low-lying Kramers doublets since at this temperature this is the only significantly populated cobalt(II) level. Therefore, the quantitative analysis of these interactions can be conveniently described by an anisotropic exchange Hamiltonian of the type (1). In

$$H_{ex} = -2J_z S_{z1} S_{z2} - 2J_{xy}(S_{x1} S_{x2} + S_{y1} S_{y2}) \qquad (1)$$

this expression S_i ($i = 1$ or 2) represents an effective spin 1/2 associated to the lowest Kramers doublet of the octahedral Co^{II}. The exchange anisotropy assumed by this model (with $J_z = J_{xy}$) comes from the large anisotropy of this low-lying spin doublet, as evidenced by EPR spectra. This anisotropic model

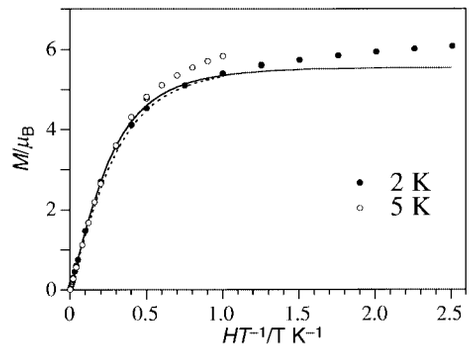

Fig. 13 Plot of the isothermal magnetisation M (per pair of cobalt(II) ions) *vs.* H/T at 2 and 5 K for complex **2**. The theoretical behaviour calculated from the parameters obtained in the fit of the magnetic susceptibility data is plotted as solid (2 K magnetisation) and dashed (5 K magnetisation) lines.

has provided a satisfactory fitting of the magnetic behaviour in the low temperature region (below 30 K). The following set of parameters has been obtained: $J_z = 2.1$ cm^{-1}, $J_z/J_{xy} = 1$ to 2, $g_z = 7.9$, $g_{xy} = 2.5$ (inset in Fig. 12). As for other cobalt(II) systems, the fitting procedure has not been an easy task due to the large number of adjustable parameters. In particular, it has shown to be largely insensitive to the amount of exchange anisotropy as we can see in the figure (dashed and solid lines). Still, this magnetic analysis has provided reliable information on the sign and magnitude of the Co^{II}–Co^{II} exchange interaction. Other complementary techniques, for example specific heat measurements, need to be employed in order precisely to determine the amount of exchange anisotropy. Furthermore, this analysis has indicated that these exchange interactions are restricted, as in the manganese derivative, to the dimeric units present in the chain. Interdimer antiferromagnetic interactions may be also present, but they remain negligible since they only affect the magnetic behaviour below 4 K. In fact, the comparison of the low temperature magnetisation data indicates that at 2 K the magnetisation curve is only slightly below that at 5 K, suggesting that quite weak antiferromagnetic interdimer interactions are operative at the lower temperature (Fig. 13).

The unusual presence of ferromagnetic coupling in these two compounds deserves explanation. In the cobalt case the result is not too surprising as the M–O–M angles within the dimeric unit are equal to 103°, which is in the range in which the Co–Co ferromagnetic pathways are dominant as a consequence of an accidental orthogonality of the magnetic orbitals that are pointing towards the bridging oxygen atoms. In fact, ferromagnetic couplings of the order of $J_z = 10$ cm^{-1} have also been observed in tetranuclear Co_4O_{16} clusters having M–O–M angles between 90 and 100°.[10] However, in the manganese derivative this kind of interaction is extremely rare as for this and for the other d^5 ions (like high-spin Fe^{III}) the five d orbitals are magnetically active and therefore some of the orbital pathways are bound to be antiferromagnetic. For example, the manganese(II) cluster which is isomorphous to the tetranuclear cobalt(II) cluster exhibits weak antiferromagnetic pairwise interactions.[11] The first precedent in which the net interaction is ferromagnetic has been provided by complexes having as bridging ligands two azido ions double bonded in an end-on (μ-(1,1)) fashion. With the azido ligand a dinuclear manganese(II) complex[12] as well as two iron(II) dimers[13,14] exhibiting weak ferromagnetic couplings have been reported. In these complexes the angles at the azido bridge are similar to that observed in our compound (105 to 107°). Recently an isophthalate-bridged manganese(II) chain complex which contains ferromagnetically coupled manganese(II) dimers with double carboxylates in *syn-syn* conformation has also been reported.[15] Nevertheless, to the best of our knowledge, the manganese(II) complex reported in the present work constitutes the first manganese(II) complex in

which the ferromagnetic coupling is transmitted through a μ-(1,1) bridging carboxylate. In this respect this compound adopts the same co-ordination mode as the end-on azide ligand, a mode that is unusual for the carboxylate ligand.

Conclusion

Six different co-ordination polymers have been prepared by hydrothermal synthesis of a polyaromatic acid with a divalent metal ion (M = Co, Mn or Zn) and 2,2′-bipyridyl. In each case a co-ordination polymer with infinite chains in one dimension only was formed as anticipated owing to the tight binding of 2,2′-bipyridyl to some or all of the metal cations. In all cases the chains 'slot together' and associate by van der Waals forces between the 2,2′-bipyridyl rings. The acids H_3TPO and H_2SDA failed to give co-ordination polymers with metal cations in hot water in the absence of 2,2′-bipyridyl which exemplifies the easier formation of 1-D *versus* 2-D or 3-D infinite lattices. This is attributed to the less directional nature of van der Waals forces and hydrogen bonding compared to the geometrical requirements of metal ion–ligand co-ordination which propagates through the infinite network. Lattices **4** and **5** incorporating BTC and TPO respectively have an open framework structure with large molecular channels occupied by disordered water molecules. Retention of the crystallinity and porosity of $[Co_3(TPO)_2(BIPY)_2(H_2O)_6]\cdot xH_2O$ **5**, after mild desorption of the non-co-ordinating water molecules, is attributed to the still fully co-ordinated metal ions. They undergo H_2O/D_2O solvent exchange characteristic of a zeolite. Further studies are in progress of the scope for rational design of acid and bidentate ligand for solid state assembly.

Experimental

All hydrothermal synthesis experiments were performed in Teflon™ lined 23 or 45 ml bombs (Parr 4749 and 4744) heated using a Heraeus Instruments oven (type 6030) fitted with a Eurotherm 902PX programmer. All infrared spectra were recorded on KBr discs using a ATI Mattson Genesis series FTIR spectrometer. Thermal gravimetric analysis was performed in an atmosphere of either flowing nitrogen gas or air, using a Stanton Redcroft STA-780 instrument. The C,H,N microanalyses were performed by Butterworth Laboratories Ltd. Cobalt microanalysis was by means of atomic absorption spectroscopy using a Varian SpectrAA-10 using an air/acetylene flame. In some cases microanalyses were performed in duplicate on separate batches to verify the sample homogeneity. Variable temperature susceptibility measurements were carried out in the temperature range 2–300 K at a magnetic field of 0.1 T on polycrystalline samples with a magnetometer (Quantum Design MPMS-XL-5) equipped with a SQUID sensor. The susceptibility data were corrected from the diamagnetic contributions as deduced by using Pascal's constant tables.

Syntheses

$[\{Mn(HBTC)(BIPY)(H_2O)\}_n]$ 1. The compounds H_3BTC (102 mg, 486 μmol), $Mn(OAc)_2\cdot 4H_2O$ (119 mg, 486 μmol), 2,2′-bipyridyl (77 mg, 493 μmol), and water (10 ml) were placed in a 23 ml bomb. The bomb was heated at 10 °C h^{-1} to 210 °C; after 2 h it was cooled to 180 °C at a rate of 5 °C h^{-1}, before being cooled at 1 °C h^{-1} to 20 °C. Compound **1** (199 mg, 94%) was collected as large yellow crystals. Found: C, 51.7; H, 3.1; N, 6.2 [$Mn(HBTC)(BIPY)(H_2O)$] = $C_{19}H_{14}MnN_2O_7$ requires C, 52.2; H, 3.2; N, 6.4%. IR 3416s, 1686s, 1655w, 1613s, 1531m, 1560m, 1496w, 1479m, 1444m, 1404w, 1371s, 1336s, 1321s, 1245m, 1185m, 1162w, 1098w, 1064w, 1019w, 1003w, 941w, 893w, 801w, 760m, 737m, 673m, 649w and 534w cm^{-1}. TGA: no significant mass loss up to 230 °C after which decomposition occurred.

$[\{Co(HBTC)(BIPY)(H_2O)\}_n]$ 2. The compounds H_3BTC (100 mg, 476 μmol), $Co(OAc)_2\cdot 4H_2O$ (120 mg, 482 μmol), 2,2′-bipyridyl (75 mg, 480 μmol) and water (10 ml) were placed in a bomb then heated at 100 °C h^{-1} to 220 °C. After holding at this temperature for 2 h the bomb was cooled at 5 °C h^{-1} to 180 °C. After 6 h at 180 °C the bomb was cooled at 5 °C h^{-1} to 100 °C and then at 6 °C h^{-1} to 20 °C. Compound **2** was collected by filtration, washed with water and air dried to give red crystals (186 mg, 89%). Found: C, 51.8(51.6); H, 3.2(3.0); N, 6.2(6.3). [$Co(HBTC)(BIPY)(H_2O)$] = $C_{19}H_{14}CoN_2O_7$ requires C, 51.7; H, 3.2; N, 6.4%. IR: 3397s, 3103m, 3092m, 3031w, 1695vs, 1655w, 1615s, 1606s, 1579s, 1564s, 1493w, 1475m, 1442m, 1411m, 1371s, 1337s, 1317m, 1246m, 1231s, 1179m, 1158m, 1100m, 1063w, 1046w, 1025w, 1014w, 1006(sh), 962w, 944w, 894m, 882w, 817w, 802m, 762s, 736m, 692m, 674s, 652m, 606w, 530m, 466w, 439w and 416m cm^{-1}. TGA: when heated in nitrogen at 2 °C min^{-1}, between 190 and 260 °C a mass loss of 4.3% occurred corresponding to dehydration of the monohydrate (4.1% theoretical).

$[\{Zn(HBTC)(BIPY)(H_2O)\}_n]$ 3. The compounds H_3BTC (101 mg, 481 μmol), $Zn(OAc)_2\cdot 2H_2O$ (105 mg, 480 μmol), BIPY (75 mg, 483 μmol), and water (20 ml) were placed in a 45 ml bomb. This was heated at 20 °C h^{-1} to 210 °C, maintained for 2 h, then cooled at 5 °C h^{-1} to 180 °C. After 6 h at 180 °C the bomb was cooled at 5 °C h^{-1} to 50 °C. From 50 to 20 °C the rate of cooling was 10 °C h^{-1}. The bomb was opened and colourless crystals of **3** were collected by filtration, washed with water and dried in air (190 mg, 88%). Found: C, 51.1(50.9); H, 2.9(2.9); N, 6.2(6.2). [$Zn(HBTC)(BIPY)(H_2O)$] = $C_{19}H_{14}N_2O_7Zn$ requires C, 51.0; H, 3.2; N, 6.3%. IR: 3410(br) s, 3088m, 1701s, 1626s, 1600m, 1584m, 1568s, 1509w, 1493w, 1477w, 1439s, 1399w, 1356vs, 1249m, 1232m, 1184m, 1103w, 1058w, 1023w, 1013w, 940w, 860w and 795w cm^{-1}. TGA: an endothermic mass loss of 3.8% was observed between 110 and 160 °C corresponding to dehydration of the monohydrate (4% theoretical); no further mass loss occurred below 290 °C after which the material decomposed.

$[Co_3(BTC)_2(BIPY)_2(H_2O)]\cdot 4H_2O$ 4. The compounds H_3BTC (100 mg, 476 μmol), $Co(OAc)_2\cdot 4H_2O$ (178 mg, 714 μmol), BIPY (113 mg, 723 μmol) and water (16 ml) were placed in a 45 ml bomb. This was heated at 100 °C h^{-1} to 180 °C, maintained for 2 h, then cooled at 5 °C h^{-1} to 20 °C. A mixture of a pink solid and blood red crystals of **4** (48 mg, 19%) was obtained. The red crystals were separated mechanically. Found: C, 44.4(44.2); H, 3.4(3.6); N, 5.2(5.1). $[Co_3(BTC)_2(BIPY)_2(H_2O)_6]\cdot 2H_2O = C_{38}H_{38}Co_3N_4O_{20}$ requires C, 43.6; H, 3.7; N, 5.4 (the solid has partially dehydrated loosing some of the non-co-ordinating H_2O molecules that were definitely observed by crystallography). IR: 3315vs(br), 1615vs, 1560s, 1492w, 1474m, 1443s, 1373vs, 1316w, 1250w, 1175w, 1158w, 1105m, 1059w, 1043w, 1024m, 930w, 816w, 762s, 732s, 653w, and 633w cm^{-1}. TGA: an endothermic mass loss of 18% was observed up to 100 °C; conversion of an octahydrate into an anhydrous solid requires a mass loss of 14%.

$[Co_3(TPO)_2(BIPY)_2(H_2O)_6]\cdot xH_2O$ 5. The compounds H_3TPO (207 mg, 505 μmol), $Co(OAc)_2\cdot 4H_2O$ (200 mg, 803 μmol), BIPY (80 mg, 512 μmol) and water (20 ml) were placed in a 45 ml bomb. This was heated at 100 °C h^{-1} to 210 °C, maintained for 2 h, then cooled at 3 °C h^{-1} to 20 °C. Compound **5** was obtained as a homogeneous red solid (324 mg, 91%) by filtration and drying in air. Found: C, 52.5; H, 3.9; N, 3.9; P, 4.2. $[Co_3(TPO)_2(BIPY)_2(H_2O)_6] = C_{62}H_{52}Co_3N_4O_{20}P_2$ requires C, 52.8; H, 3.7; N, 4.0; P, 4.4%. IR: 3397(br) s, 3111w, 3093w, 3045w, 1693w, 1598m, 1541m, 1499w, 1474w, 1443w, 1425m, 1385s, 1314w, 1251w, 1164w, 1136w, 1111m, 1087w, 1080w, 1019m, 862w, 828w, 768m, 739m, 700(sh), 653w, 635w, 585w, 561w, 493w and 425w cm^{-1}. TGA: between 40 and 170 °C three

overlapping endothermic mass losses totalling 9.6% occurred; conversion of the octahydrate into an anhydrous solid requires a mass loss of 10%.

[Co(SDA)(BIPY)(H_2O)] 6. The compounds *cis*-H_2SDA (103 mg, 384 μmol), $Co(OAc)_2 \cdot 4H_2O$ (96 mg, 385 μmol), BIPY (60 mg, 384 μmol) and water (10 ml) were placed in a 23 ml bomb. This was heated at 100 °C h^{-1} to 220 °C, held for 2 h, then cooled at 5 °C h^{-1} to 180 °C. After 6 h at 180 °C the bomb was cooled at 5 °C h^{-1} to 100 °C and then at 6 °C h^{-1} to 20 °C. Large orange needle-shaped crystals were collected by filtration, washed with saturated aqueous $NaHCO_3$, then with water followed by drying in air (171 mg, 89%). Found: C, 62.6; H, 4.0; N, 5.6. [Co(SDA)(BIPY)(H_2O)] = $C_{26}H_{20}CoN_2O_5$ requires C, 62.5; H, 4.0; N, 5.6. IR: 3404(br), 3105m, 3077w, 3055m, 3043w, 3034w, 3008m, 1602s, 1577s, 1550s, 1520s, 1490m, 1473m, 1440s, 1427s, 1412vs, 1358vs, 1314m, 1277w, 1263w, 1248m, 1187w, 1175w, 1154w, 1137w, 1118w, 1105w, 1057w, 1020m, 982w, 908(sh), 897m, 868(sh), 859m, 850(sh), 836w, 800m, 781w, 764s, 732s, 699m, 652w, 629w, 598w, 584w, 563w, 552w, 529w, 483w, 430w, 417m and 403m cm^{-1}. TGA: an endothermic mass loss of 3.4% was observed between 140 and 190 °C corresponding to dehydration of the monohydrate (theoretical 3.6%). An attempt at using a mixture of *cis*- and *trans*-H_2SDA in the reaction gave a mixture of **6** and some recovered starting material.

Acknowledgements

We are grateful to the Leverhulme Trust for financial support.

References

1 (*a*) M. Fujita, Y. Kwon, S. Washizu and K. Ogura, *J. Am. Chem. Soc.*, 1994, **116**, 1151; (*b*) T. Sawaki, T. Dewa and Y. Aoyama, *J. Am. Chem. Soc.*, 1998, **120**, 8539; (*c*) P. J. Zapf, C. J. Warren, R. C. Haushalter and J. Zubieta, *Chem. Commun.*, 1997, 1543; (*d*) H. A. Brison, T. P. Pollagi, T. C. Stoner, S. J. Geib and M. D. Hopkins, *Chem. Commun.*, 1997, 1263; (*e*) C. M. Drain, F. Nifiatis, A. Vasenko and J. D. Batteas, *Angew. Chem.*, 1998, **110**, 2478; *Angew. Chem., Int. Ed.*, 1998, **37**, 2344; (*f*) S. O. H. Gutschke, M. Molinier, A. K. Powell, R. E. P. Winpenny and P. T. Wood, *Chem. Commun.*, 1996, 823.

2 (*a*) O. M. Yaghi, H. Li and T. L. Groy, *Inorg. Chem.*, 1997, **36**, 4292; (*b*) S. R. Batten, B. F. Hoskins and R. Robson, *J. Am. Chem. Soc.*, 1995, **117**, 5385; (*c*) O. M. Yaghi, G. Li and H. Li, *Nature* (*London*), 1995, **378**, 703; (*d*) R. H. Groeneman, L. R. MacGillivray and J. L. Atwood, *Chem. Commun.*, 1998, 2735; (*e*) S. Subramanian and M. J. Zaworotko, *Angew. Chem.*, 1995, **107**, 2295; *Angew. Chem., Int. Ed. Engl.*, 1995, **34**, 2127; (*f*) C. J. Kepert, D. Hesek, P. D. Beer and M. J. Rosseinsky, *Angew. Chem.*, 1998, **110**, 3335; *Angew. Chem., Int. Ed.*, 1998, **37**, 3158; (*g*) C. J. Kepert and M. J. Rosseinsky, *Chem. Commun.*, 1998, 31; (*h*) M. Kondo, T. Yoshitomi, K. Seki, H. Matsuzaka and S. Kitagawa, *Angew. Chem.*, 1997, **109**, 1844; *Angew. Chem., Int. Ed. Engl.*, 1997, **36**, 1725; (*i*) H. Li, C. E. Davis, T. L. Groy, D. G. Kelley and O. M. Yaghi, *J. Am. Chem. Soc.*, 1998, **120**, 2186; (*j*) O. M. Yaghi and H. Li, *J. Am. Chem. Soc.*, 1995, **117**, 10401; (*k*) M. J. Plater, M. R. St. J. Foreman and A. M. Z. Slawin, *J. Chem. Res.*, 1999, (*S*) 74; (*M*) 0728.

3 (*a*) M. J. Plater, A. J. Roberts and R. A. Howie, *Chem. Commun.*, 1997, 893; (*b*) M. J. Plater, A. J. Roberts, J. Marr, E. E. Lachowski and R. A. Howie, *J. Chem. Soc., Dalton Trans.*, 1998, 797.

4 (*a*) O. M. Yaghi, H. Li and T. L. Groy, *J. Am. Chem. Soc.*, 1996, **118**, 9096; (*b*) O. M. Yaghi, C. E. Davis, G. Li and H. Li, *J. Am. Chem. Soc.*, 1997, **119**, 2861; (*c*) T. M. Reineke, M. Eddaoudi, M. Fehr, D. Kelley and O. M. Yaghi, *J. Am. Chem. Soc.*, 1999, **121**, 1651.

5 (*a*) N. Yoshida, H. Oshio and T. Ito, *Chem. Commun.*, 1998, 63; (*b*) E. Ishow, A. Gourdon and J.-P. Launay, *Chem. Commun.*, 1998, 1909; (*c*) H.-P. Wu, C. Janiak, L. Uehlin, P. Klufers and P. Mayer, *Chem. Commun.*, 1998, 2637; (*d*) I. M. Muller, T. Rottgers and W. S. Sheldrick, *Chem. Commun.*, 1998, 823; (*e*) H.-P. Wu, C. Janiak, G. Rheinwald and H. Lang, *J. Chem. Soc., Dalton Trans.*, 1999, 183; (*f*) B.-H. Ye, X.-M. Chen, G.-Q. Xue and L.-N. Ji, *J. Chem. Soc., Dalton Trans.*, 1998, 2827.

6 SMART system and hemisphere data collection. All structures were solved by direct methods and refined against F^2 using SHELXTL, Version 5.01, Bruker AXS, Madison, WI, 1995.
CCDC reference number 186/1671.
See http://wwtw.rsc.org/suppdata/dt/1999/4209/ for crystallographic files in .cif format.

7 W. Chou and M. Pomerantz, *J. Org. Chem.*, 1991, **56**, 2762.

8 C. J. Kepert and M. J. Rosseinsky, *Chem. Commun.*, 1999, 375.

9 R. L. Carlin, *Magnetochemistry*, Springer, New York, 1983.

10 C. J. Gómez-García, E. Coronado and J. J. Borrás-Almenar, *Inorg. Chem.*, (*a*) 1992, **31**, 1667; (*b*) 1997, **36**, 2244.

11 C. J. Gómez García, E. Coronado, P. Gómez-Romero and N. Casañ-Pastor, *Inorg. Chem.*, 1993, **32**, 3378.

12 R. Cortés, J. L. Pizarro, L. Lezama, M. L. Arriortua and T. Rojo, *Inorg. Chem.*, 1994, **33**, 2697.

13 G. De Munno, T. Poerio, G. Viau, M. Julve and F. Lloret, *Angew. Chem., Int. Ed. Engl.*, 1997, **36**, 1459.

14 K. R. Reddy, M. V. Rajasekharan and J. P. Tuchagues, *Inorg. Chem.*, 1998, **37**, 5978.

15 X. S. Tan, J. Sun, D. F. Xiang and W. X. Tang, *Inorg. Chim. Acta*, 1997, **255**, 157.

Paper 9/05332H